Struct Bond (2016) 167: 139–162
DOI: 10.1007/430_2014_147

Published online: 10 May 2014

d^{10}-ML_2 Complexes: Structure, Bonding, and Catalytic Activity

Lando P. Wolters and F. Matthias Bickelhaupt

Abstract Our goal in this chapter is to show how one can obtain a better understanding of the decisive factors for the selectivity and efficiency of catalytically active metal complexes. This ongoing research project has been designated the 'Fragment-oriented Design of Catalysts' and aims at providing design principles for a more rational development of catalysts. To this end, we have performed a series of studies in which we systematically investigate the effect of a specific variation on the reactivity of the catalyst. Thus, we will summarize previous results on not only how the reaction barrier varies when different bonds are activated by palladium, different ligands are attached to palladium but also how different metal centers perform compared to palladium. In a final section, we present a case study on newly obtained results about the effect of adding substituents with different electronegativity to the phosphine ligands at the metal center. A red thread throughout the chapter, and our methodology in general, is the application of the activation strain model of chemical reactivity. This is a predictive model that provides a quantitative relationship between trends in barrier heights and variation of geometric and electronic properties of the reactants.

Keywords Activation strain model · Bond activation · Bond theory · Catalysis · Density functional calculations · Halogenated phosphine ligands · Ligands · Transition metal complexes

L.P. Wolters
Department of Theoretical Chemistry and Amsterdam Center for Multiscale Modeling, VU University, De Boelelaan 1083, 1081 HV Amsterdam, The Netherlands

F.M. Bickelhaupt (✉)
Department of Theoretical Chemistry and Amsterdam Center for Multiscale Modeling, VU University, De Boelelaan 1083, 1081 HV Amsterdam, The Netherlands

Institute for Molecules and Materials, Radboud University Nijmegen, Heyendaalseweg 135, 6525 AJ Nijmegen, The Netherlands
e-mail: F.M.Bickelhaupt@vu.nl

Contents

1 Introduction

In an era of growing concern about the human energy demands and its consequences for the environment, the importance of catalysis is evident. One of the most ubiquitous families of catalytic cycles is that of cross-coupling reactions [1, 2]. These catalytic cycles can be applied to form carbon–carbon bonds, which are of paramount importance for the synthesis of pharmaceuticals, as well as materials. The active catalytic species in these cross couplings is a transition metal complex, often based on palladium (Scheme 1). The ongoing importance of palladium-catalyzed cross-coupling reactions has been emphasized by the fact that it was the topic of the 2010 Nobel Prize in chemistry [3–5].

Cross-coupling reactions are initiated by the oxidative addition of a substrate (typically an aryl halide) to the ligated palladium complex PdL_n. This first step is generally considered to be important for both the efficiency and selectivity of the process, and is therefore widely studied both experimentally [6–10] and theoretically [11–14]. Although this vast body of work has certainly contributed to the understanding of catalytic reactivity, it is still hard to predict the reactivity of a complex, due to the many available variables, such as metal center, ligands, substrate, solvent, and reaction conditions. Not only insight into the effect of all these variables is required, but also the interplay between all these effects has to be understood in order to make reliable predictions. Therefore, despite the huge amount of available literature, the actual catalyst selection process is still often done through a process based on experience and trial and error. In order to facilitate this selection process, we employ theoretical chemistry, which allows variation of one parameter at a time, under strictly controlled conditions and without any experimental limitation, while simultaneously the added benefit of available analysis tools allows us to explain the observed effects and eventually their interplay. This strategy of gradually building up insight into the catalytic activity has been termed the ‘Fragment-oriented Design of Catalysts’ [15], and aims at allowing

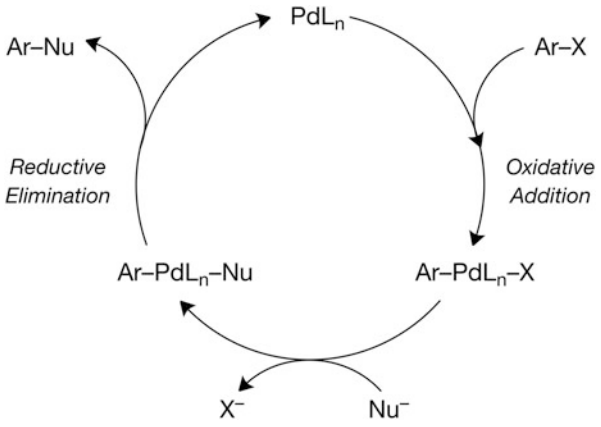

Scheme 1 Schematic catalytic cycle for a palladium-catalyzed cross coupling

chemists in the future to rationally design catalysts with the desired selectivity and optimized efficiency.

In this work, we will briefly discuss a selection of previously obtained insights, either by us or by other groups, as well as newly obtained results on palladium complexes with halogenated phosphine ligands. This case study serves as an instructive example of a study on reactivity, as well as its connection with molecular geometry and bond analyses. To explain the insights, we apply the activation strain model of chemical reactivity [16–19], which we will therefore discuss first. This model, combined with an interaction energy decomposition and qualitative molecular orbital (MO) theory, explains trends in reaction barriers and reaction energies, and it elucidates the bonding mechanism between molecular fragments. Note that this additional insight does not replace but comes on top of a computational quest for the most feasible among several plausible reaction pathways, including unwanted side reactions. Note also that to optimize a catalyst for a specific process, one must consider the complete catalytic cycle, including not only the overall reaction barrier but also the consequences of the stabilization of intermediates for which an energy span model, based on the steady-state approximation, has been developed [20–23].

2 The Activation Strain Model of Chemical Reactivity

The activation strain model of chemical reactivity [16–19] is a fragment-based approach to understand (trends in) chemical reactivity, in terms of the intrinsic properties of reference fragments. Due to its fragment-based nature, the model is most often applied to bimolecular processes, such as oxidative additions [24] as in this work, but also S_N2-reactions [16, 25, 26], pericyclic reactions [27], and even barrier-free bond formations, such as hydrogen or halogen bonds [28]. However, also unimolecular processes are successfully studied using the activation strain

model [29–31]. Since we are in this work primarily interested in the oxidative-addition reaction, we will discuss the activation strain model as it is most commonly applied to a bimolecular process, with the fragments chosen to be the two reactants: the catalyst and the substrate.

Starting from two isolated reference fragments, the oxidative addition involves the deformation of, and interaction between, the catalyst and the substrate. Within the activation strain model, the relative energy ΔE at a certain point of the reaction energy profile (plotted along the reaction coordinate ζ) is split accordingly into two terms. The first term is the strain energy, ΔE_{strain}, that is associated with the deformation energy of the fragments from their reference geometries to the geometry they acquire at the point of interest, and eventually also accounting for electronic excitations or relaxations. The second term, the interaction energy ΔE_{int}, accounts for all mutual chemical interactions between these deformed fragments [Eq. (1)].

$$\Delta E(\zeta) = \Delta E_{\text{strain}}(\zeta) + \Delta E_{\text{int}}(\zeta). \tag{1}$$

To obtain insightful results, it is important to choose a proper reaction coordinate. For oxidative additions, the elongation of the bond that is broken has been shown to be a suitable parameter to project the reaction coordinate onto [32]. The activation strain analyses in the present work are therefore projected onto the stretch of the activated bond. The strain energy can be divided into contributions ΔE_{strain}[cat] from the catalyst and ΔE_{strain}[sub] from the substrate. The interaction energy ΔE_{int} can be analyzed in the conceptual framework provided by the Kohn–Sham molecular orbital method [33, 34]. It can be further divided into three physically meaningful terms [Eq. (2)], using a quantitative energy decomposition scheme developed by Ziegler and Rauk [33, 35].

$$\Delta E_{\text{int}}(\zeta) = \Delta V_{\text{elstat}}(\zeta) + \Delta E_{\text{Pauli}}(\zeta) + \Delta E_{\text{oi}}(\zeta). \tag{2}$$

The term ΔV_{elstat} corresponds to the classical electrostatic interaction between the unperturbed charge distributions $\rho_{\text{A}}(r)+\rho_{\text{B}}(r)$ of the prepared or deformed fragments A and B that adopt their positions in the overall molecule AB, and is usually attractive. The Pauli repulsion term ΔE_{Pauli} comprises the destabilizing interactions between occupied orbitals and is responsible for the steric repulsion (see Fig. 1). This repulsion is caused by the fact that two electrons with the same spin cannot occupy the same region in space. It arises as the energy change associated with the transition from the superposition of the unperturbed electron densities $\rho_{\text{A}}(r)+\rho_{\text{B}}(r)$ of the geometrically deformed but isolated fragments A and B, to the wavefunction $\Psi^0 = N\hat{A}[\Psi_{\text{A}}\Psi_{\text{B}}]$, that properly obeys the Pauli principle through explicit antisymmetrization ($\hat{A}$ operator) and renormalization (N constant) of the product of fragment wavefunctions (see [33] for an exhaustive discussion). The orbital interaction ΔE_{oi} accounts for electron pair bond formation, charge transfer (interaction between occupied orbitals on one fragment with unoccupied orbitals on the other fragment, including the HOMO–LUMO interactions), and

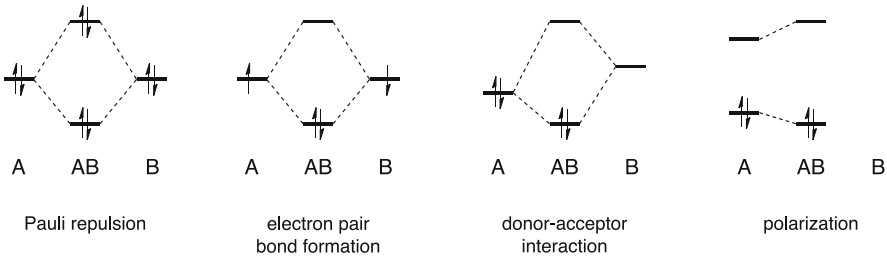

Fig. 1 Schematic representations of Pauli repulsion, and some commonly encountered interactions (electron pair bond formation, donor–acceptor interactions and polarization) contributing to the orbital interaction energy

polarization (empty–occupied orbital mixing on one fragment due to the presence of another fragment). Schematic representations of these interactions are shown in Fig. 1. The orbital interaction term can be further divided into contributions from each irreducible representation Γ of the interacting system [see Eq. (3)].

$$\Delta E_{\mathrm{oi}}(\zeta) = \sum\nolimits_{\Gamma} \Delta E_{\mathrm{oi}}^{\Gamma}(\zeta). \tag{3}$$

When applied to dispersion-corrected computations, Eq. (2) can be augmented with a term ΔE_{disp}.

With regard to the activation strain model of chemical reactivity and the interaction energy decomposition analyses, it should be noted that the former can be applied using any quantum chemistry software package, whereas the quantitative energy decomposition scheme is a unique feature of the Amsterdam Density Functional program package (ADF) [36–38]. The PyFrag program has been developed as a wraparound for ADF, to streamline performing the activation strain analyses [39].

3 Fragment-Oriented Design of Catalysts

3.1 Activation of Different Bonds

In order to understand the activity of a catalyst, one must first have a decent understanding of the reaction mechanism. To this end, studies have been performed on the activation of a number of different bonds by the most simple model catalyst: a bare Pd(0) atom. This enables one to understand the intrinsic reactivity of the metal atom and how the reaction barrier for oxidative addition is influenced by the different bonds to be activated [17, 18, 40–43]. It was found that the $d^{10}s^0$ occupation of the metal is of great importance for the oxidative-addition reaction, because charge donation from the occupied metal d orbitals into the substrate's σ* orbital is

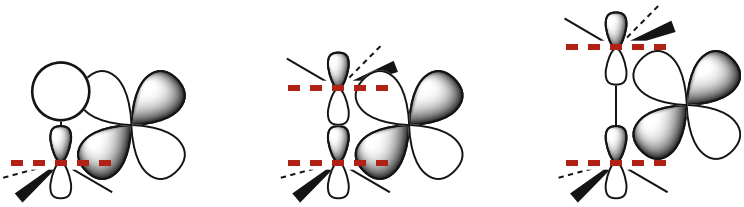

Fig. 2 Different overlap situations for the metal d orbital with a C–H bond (*left*), a C–C bond (*middle*), and with a stretched C–C bond (*right*)

the driving force behind the reaction, while the empty metal s orbital allows the substrate to coordinate to the metal center. To explain the reactivity of Pd(0) towards different bonds, the bond dissociation energy of these bonds is, of course, one of the key factors determining the height of the reaction barrier. For example, addition of halomethanes CH_3X with X=F, Cl, Br, I and At goes with decreasing reaction barriers from F to At [42]. This trend results directly from the decreasing C–X bond strength that is observed in CH_3X along this series.

However, the strength of the bond to be activated is not the only factor that determines the height of the reaction barrier. It is known, for example, that activation of the stronger methane C–H bond can be kinetically more feasible than activation of a weaker ethane C–C bond [44–47]. This has been attributed to the different compositions of the antibonding σ* acceptor orbital [43, 45, 48]. For the C–H bond, this orbital is the antibonding combination of the methyl sp^3 lobe and the 1s orbital on hydrogen, whereas for the C–C bond it is the antibonding combination of two methyl sp^3 lobes. The latter combination has an additional nodal plane, and the C–C bond therefore has to stretch further in order to achieve favorable overlap (avoid cancellation of overlap) with the metal d orbitals (Fig. 2). This leads to a delay in the buildup of stabilizing catalyst–substrate interactions and therefore a destabilization of the transition state. In the activation strain model, this shows up as a ΔE_{int} term that starts to become more stabilizing only at a later stage, while the destabilizing term ΔE_{strain} is already increasing considerably at an early stage of the reaction. A similar effect is found for carbon–halogen bonds C–X, where the σ* orbital is composed of an antibonding combination of the methyl sp^3 hybrid and the halogen p orbital. Furthermore, for ethane C–C activation, the strain energy is additionally destabilized because of the need to bend two methyl groups away in order to make room for the metal, instead of only one methyl group in the case of methane.

3.2 The Effect of Ligand Variation

A logical next step towards more applicable reactions is to study the effect of adding ligands to the palladium center. Firstly, we will discuss the effect of adding a

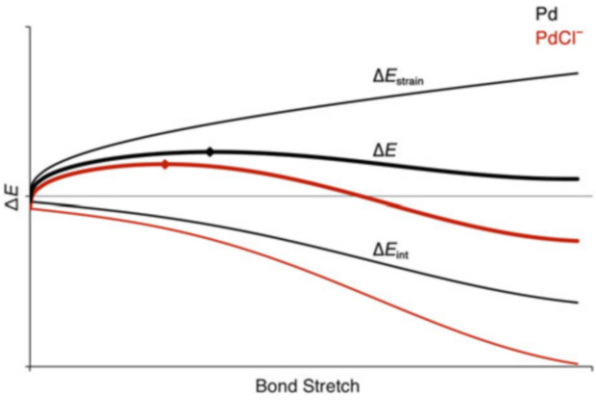

Fig. 3 Schematic comparison of the activation strain analyses obtained for bond activation by Pd(0) (*black*) and anion-assisted $PdCl^-$ (*red*). For clarity, the strain curves are coincident, which is a valid approximation for most practical applications

chloride ligand [17]. The effect of adding an anion is known to be able to speed up oxidative-addition reactions to zerovalent palladium complexes, as well as, for example, the rate-determining step in the industrially important Monsanto process [49–53]. By directly comparing activation of H–H, C–H, C–C, and C–Cl bonds by Pd as well as $PdCl^-$, such anion assistance was shown to decrease all oxidative addition barriers. Expectedly, adding a chloride anion to the palladium center has not much effect on the strain energy (ΔE_{strain}) curve, which for all reactions closely resembles the bond dissociation profile. The reason for the lower reaction barriers is a substantially stabilized catalyst–substrate interaction ΔE_{int} (Fig. 3). This strengthening becomes larger as the reaction proceeds, because the inherent strength of the catalyst–substrate interaction also increases along the reaction profile. Therefore, the interaction energy profile descends more steeply, shifting the position of the TS to the left. This implies that the transition state is more reactant-like as the exothermicity of the reaction is increased, which is reminiscent of the Hammond postulate [54]. Thus, the origin and mechanism of this postulate emerges naturally in terms of the activation strain model. A further quantitative decomposition of the interaction energy [see Sect. 2 and Eq. (2)] along the energy profile shows that the stronger interaction results from a less destabilizing Pauli energy term, which constitutes the repulsive interactions between occupied orbitals on the fragments (see Fig. 1). These interactions are weakened due to the greater orbital energy gap between the occupied orbitals on $PdCl^-$ and those on the substrate. The orbitals of $PdCl^-$ are pushed up in energy due to the presence of the negatively charged chloride. The higher occupied catalyst orbitals also strengthen the backbonding interactions to the substrate, but this contribution is masked by the decreased substrate-to-metal donation because also the catalysts' acceptor orbitals are destabilized.

The situation changes considerably when dicoordinated species are studied, such as the bisphosphine complex $Pd(PH_3)_2$. Compared to bare Pd or monocoordinated palladium complexes, the barriers for oxidative addition to dicoordinated complexes are significantly higher [55–59]. Activation strain analyses revealed [57] that the main reason for the higher reaction barriers is an increased catalyst strain energy

ΔE_{strain}[cat], that results from the need of bending the ligands away to avoid steric repulsion with the substrate. This destabilizing effect due to the need to decrease the ligand–metal–ligand angle (the bite angle) can be avoided by bending the catalyst in advance, as, for example, in chelate complexes Pd[$PH_2(CH_2)_nPH_2$] where the bite angle can be controlled by varying the length of the carbon-chain $(CH_2)_n$. It is well known that the reactivity of a catalytic complex depends on its bite angle [21, 60–64]. By studying oxidative addition of several bonds to this series of model catalysts with $n = 2$–6, bite angles from 98° to 156° can be achieved, and a clear relationship was found between the ligand–metal–ligand angles and the activation barriers. Upon decreasing the length of the carbon-chain in the bidentate ligand, the bite angle decreases, and concomitantly the activation barrier is lowered as a result of the less strong destabilizing catalyst strain energy ΔE_{strain}[cat], because there is less need to deform the catalyst. In other words: part of the strain energy is taken out of the reaction energy profile by building it into the catalytically active complex. This steric mechanism is the main reason for the lower reaction barriers for oxidative addition to catalytic complexes with smaller bite angles. It is, however, accompanied by a small electronic effect, namely the enhanced backbonding from a destabilized palladium d orbital to the substrate σ* orbital. In the past it has been suggested by Hofmann and co-workers that this electronic nature was the main reason for the lower barriers for catalysts with smaller bite angles [65]. Although this electronic effect contributes to their increased reactivity, it is marginal compared to the steric effect.

3.3 The Effect of Metal Variation

Yet another parameter to be varied is the metal center itself. Although palladium is widely used, it is not used exclusively. Examples are the rhodium-based catalyst in the already mentioned Monsanto process, but also nickel, platinum, and even gold complexes have been found to be active species [6, 10, 12, 66–68]. In our group, we have studied the activation of C–H, C–C, C–F, and C–Cl bonds by the bare coinage metal cations Cu^+, Ag^+, and Au^+ and compared the results to those of Pd [69]. It was found that in general the second-row elements Pd and Ag^+ have the highest barrier towards bond activation. Even though the barriers for addition to the group 11 cations can be rather similar to the barriers for palladium, the bonding mechanism is different. Upon comparing the activation strain analyses for palladium with those of the group 11 cations (Fig. 4), three observations are easily made: firstly, and expectedly, the strain curves hardly change as there is no ΔE_{strain}[cat] and ΔE_{strain}[sub] is not significantly influenced by the metal center. Secondly, the interaction curves for the group 11 cations start at a lower energy, but are more shallow than for palladium. Thirdly, and as a result of the more shallow interaction energy curves, the reactant side of the energy profile for the cations is stabilized compared to palladium, while the product side is less stabilized or even destabilized, thereby shifting the TS to a more product-like geometry (Fig. 4).

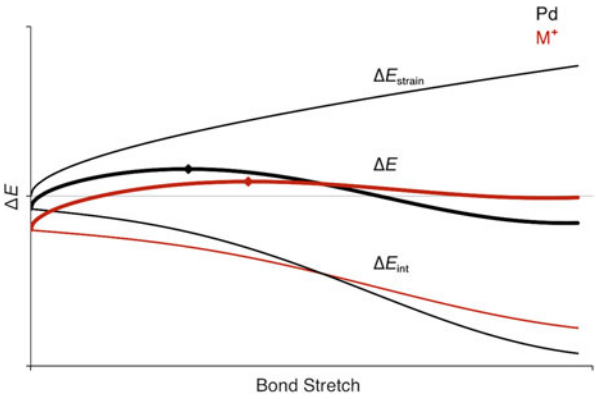

Fig. 4 Schematic comparison of the activation strain analyses obtained for bond activation by Pd(0) (*black*) and a bare cation M^+ (*red*). For clarity, the strain curves are coincident, which is a valid approximation for most practical applications

The reason for the more shallow interaction energy curves for the group 11 cations is easy to understand when one considers the different bonding interactions during the oxidative addition process. At the initial stage, the dominant interaction is donation from the substrate into the empty metal s orbital, while at a later stage backdonation from the metal d orbitals into the substrate σ* orbital becomes the most important bonding interaction. The cations, due to their net positive charge, are excellent electron acceptors, which enhances the bonding interactions in the initial stage. For the same reason, they are less good electron donors, resulting in a weaker backbonding interaction at a later stage.

These results are confirmed by a recent follow-up study on the addition of the methane C–H bond to a more extensive set of d^{10} transition metal complexes [70]. In this study, all transition metals surrounding palladium in the periodic table were included, as well as mono- and dicoordinated complexes ML and ML_2, where L is either NH_3, PH_3, or CO. In this work, all reaction profiles were analyzed with respect to the metal in its $d^{10}s^0$ configuration, which means that the catalysts based on the group 9 metal centers Co, Rh, and Ir are negatively charged, whereas the catalysts based on the group 11 metals are, as in the previous study, positively charged. For some catalysts the $d^{10}s^0$ configuration (or $d^{10}s^0$-like when ligands are present) is an excited state, but using the same electronic configuration for all complexes allowed us to make a consistent comparison of the metal centers. Furthermore, this $d^{10}s^0$ or $d^{10}s^0$-like configuration corresponds to the ground state of most catalysts used in practice.

Upon comparison of the energy profiles of, for example, $Rh(PH_3)_2^-$, $Pd(PH_3)_2$, and $Ag(PH_3)_2^+$, it was found that the methane addition barrier generally increases from anionic to cationic complexes. Activation strain analyses, a further interaction energy decomposition and detailed molecular orbital analyses revealed that this is due to poorer backbonding capabilities of the catalytic complex, which lead to a less stabilizing interaction energy term, while there is less variation among the strain energy curves. Furthermore, it was found that also in the group 9 and group 10 triads of metals the catalysts based on the second-row transition metal generally have the highest barrier towards methane activation. Again, the strain energy curves

only showed minor differences, and the main reason for this trend is a similar trend in the interaction energy curves. Thus, the catalysts with first- and third-row transition metal centers both have a more stabilizing interaction with the substrate than the second-row transition metal, albeit for different reasons. Compared to the second-row metal centers, the first row metals typically have higher-energy d orbitals (when comparing the relevant $d^{10}s^0$ configurations), which results in stronger backbonding capabilities and therefore lower energy profiles. The second and third row transition metal centers, on the other hand, have similar d orbital energies, but the latter have larger orbitals which show greater overlap with the substrate σ* orbital, leading to slightly improved backbonding. This is accompanied by the relativistic stabilization of the third row metal $(n+1)$s orbital, which results in better electron-accepting capabilities of the catalytic complex and hence a stronger substrate-to-metal donation.

The differences in catalyst strain energy that were found along this series, as well as the series from $Rh(PH_3)_2^-$ to $Ag(PH_3)_2^+$, resulted from variations in flexibility of the ligand–metal–ligand angle of the catalyst, as has been briefly touched upon before [57]. For example, from $Rh(PH_3)_2^-$ to $Pd(PH_3)_2$ to $Ag(PH_3)_2^+$ the decreased flexibility contributes to the higher barriers. We found that many catalysts have very flat potential energy surfaces for bending the bite angle, and in fact, some ML_2 complexes even have nonlinear equilibrium geometries. This leads us to additional research [71] on the geometries and bonding mechanism of such ML_2 complexes, the results of which are discussed in the next section.

3.4 Nonlinear d^{10}-ML_2 Transition Metal Complexes

In general, d^{10}-ML_2 transition metal complexes are expected to have linear L–M–L angles [72–75], which can be easily rationalized in terms of several models, among which the Walsh diagrams based on MO theory [76]. The main bonding interaction is considered to be σ donation from the ligand lone-pair orbitals into the empty metal $(n+1)$s atomic orbital, which has a bond overlap that is independent of the ligand–metal–ligand angle. The geometries of ML_2 complexes are therefore expected to be linear, due to steric interactions between the ligands, pushing them as far apart as possible. However, nonlinear geometries are observed for some complexes, such as $Ni(CO)_2$ [77, 78]. In a study on a large set of d^{10}-ML_2 complexes, with M = Co^-, Rh^-, Ir^-, Ni, Pd, Pt, Cu^+, Ag^+ Au^+ and L = NH_3, PH_3 or CO, we have shown that the equilibrium geometries deviate increasingly from linearity when the ligand is a better π-acceptor, and also when the metal is a better electron donor [71]. Thus, from NH_3- to PH_3- to CO-ligated catalysts, the nonlinearity increases, as, for example, shown by $Rh(NH_3)_2^-$ (180°), $Rh(PH_3)_2^-$ (141°), and $Rh(CO)_2^-$ (131°). Furthermore, as along the iso-electronic series of complexes from $Ag(CO)_2^+$ to $Pd(CO)_2$ to $Rh(CO)_2^-$ the electron-donating capability of the metal center increases, the nonlinearity increases as well: whereas $Ag(CO)_2^+$ is linear, $Pd(CO)_2$ has an angle of 156° and $Rh(CO)_2^-$ of 131°.

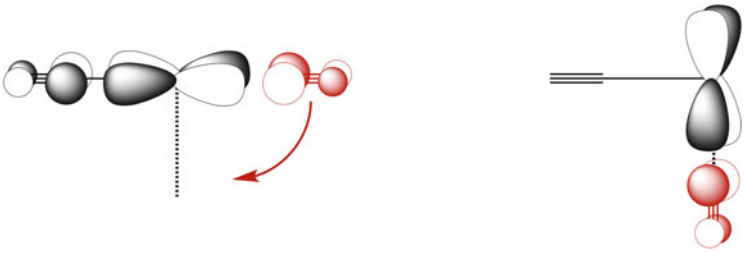

Fig. 5 Schematic representation of the π-backbonding interactions in d^{10}-ML_2 complexes at 180° and 90°. Figure adapted from [71]

A detailed analysis of the bonding mechanism of these intrinsically bent catalytic complexes has shown that π-backbonding plays a critical role in arriving at this geometric preference, as suggested by the two trends just described. Thus, we have analyzed the bonding mechanism between a monocoordinated ML fragment and the second ligand L′ while varying the L–M–L′ angle from 180° to 90°. It was found that, upon bending, the bonding interactions between LM and L′ become stronger due to increased π-backbonding, while simultaneously, as expected, the steric repulsion between the fragments strengthens as well. The reason for this enhanced π-backbonding is easy to understand in terms of the changing orbital interactions between the fragments as the L–M–L′ angle is bent: in the linear geometry, the two degenerate π-accepting orbitals on L′ interact with d-derived orbitals on LM that are already stabilized due to π-backbonding within LM. When the angle is decreased, the overlap between one π* orbital on L′ and the bonding orbital on LM is decreased, while simultaneously this same π* orbital builds up overlap with a non-bonding, essentially pure d orbital on the metal fragment (Fig. 5). This latter orbital has no bonding interactions with the first ligand L and is therefore higher in energy, which favors the π-backdonation to the second ligand L′. If this additional stabilization is stronger than the increased steric repulsion, the minimum on the energy profile shifts towards angles smaller than 180°, leading to nonlinear equilibrium geometries.

This gain in stabilization is strongest when the intrinsic π-backbonding is strongest, that is, when the metal is a better electron donor, or when the ligand is a better π-acceptor. Therefore, the catalytic complexes are more strongly bent along $Ag(CO)_2^+$, $Pd(CO)_2$, and $Rh(CO)_2^-$ and along $Rh(NH_3)_2^-$, $Rh(PH_3)_2^-$, and $Rh(CO)_2^-$.

Furthermore, we also noted that going down the periodic table, for example from $Ni(CO)_2$ to $Pd(CO)_2$ to $Pt(CO)_2$, the complexes become more linear. This is attributed to, firstly, a weaker π-backbonding for $Pd(CO)_2$ than for $Ni(CO)_2$, because the palladium 4d orbitals are lower in energy than the nickel 3d orbitals (again, analyses are relative to the $d^{10}s^0$ configuration, which is not the atomic ground state for Ni). Secondly, from $Pd(CO)_2$ to $Pt(CO)_2$ the steric repulsion upon bending becomes stronger due to a stronger admixture of the relativistically stabilized platinum 6s orbital with the occupied d_{z^2} orbital on the ML fragment. This leads to an enlarged torus of the d_{z^2} orbital, and upon bending towards 90°, an increased repulsive overlap of this torus with the lone pair on the ligand.

Although the arguments presented here are developed for d^{10}-ML_2 complexes, similar arguments account for the nonlinear structures observed for d^0 metal complexes with π-donating ligands [79–83]. Furthermore, similar reasoning is expected to account for a related effect described for d^8-$M(CO)_2L_2$ complexes by Eisenstein and Caulton, where strong π-accepting ligands induce non-planarity [84, 85].

4 Case Study: Halogenated Phosphine Ligands at Palladium

4.1 Introduction

In this section we will present newly obtained results on the activation of the methane C–H bond by halogen-substituted palladium-phosphine complexes $Pd(PX_3)_2$ where X=F, Cl, Br, or I. This topic has been briefly touched upon in previous work by us [57] as well as others [55], but these studies only included $Pd(PCl_3)_2$. Here, we will therefore discuss not only the difference in reactivity upon going from $Pd(PH_3)_2$ to halogen-substituted $Pd(PX_3)_2$ but also the effect of decreasing electronegativity along $Pd(PF_3)_2$, $Pd(PCl_3)_2$, $Pd(PBr_3)_2$, and $Pd(PI_3)_2$, which is new. Furthermore, as the bulkiness of the ligands increases from PH_3 to PF_3, PCl_3, PBr_3, and PI_3, we do not only expect electronic effects to play a role, but steric effects as well. Thus, by studying the reactivity of this series of catalysts, we investigate both electronic and steric effects on catalytic activity. However, because in a previous study [57] the $Pd(PCl_3)_2$ complex was found to have a nonlinear equilibrium geometry (a feature that was overlooked by Fazaeli and co-workers [55]),[1] we will first perform detailed bonding analyses to investigate the reasons behind this nonlinearity of $Pd(PCl_3)_2$ and compare its situation to the other halogenated phosphine-catalysts in this series. Interestingly, the latter appear to have nonlinear geometries as well. Furthermore, we will also compare these findings to the results discussed in Sect. 3.4.

4.2 M–L Bonding Analysis and $Pd(PX_3)_2$ Geometries

Our dispersion-corrected computations at ZORA-BLYP-D3/TZ2P (the computational details are described in [62], except that we have now also included dispersion corrections using Grimme's third-generation DFT-D3 method, as described in [86]) revealed that all halogen-substituted bisphosphine palladium complexes

[1] We have performed a geometry optimization of $Pd(PCl_3)_2$ at the computational level described in reference 49, resulting in a P–Pd–P angle of 135.5°. We find that the linear conformer is 1.4 kcal mol^{-1} higher in energy, with two degenerate imaginary frequencies, both corresponding to bending the complex.

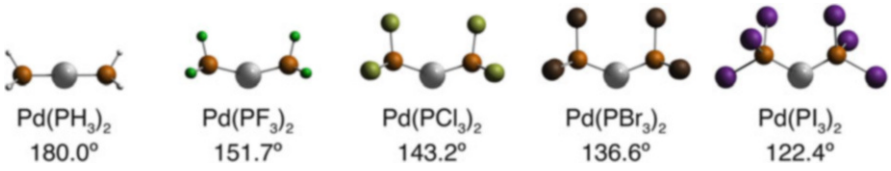

Fig. 6 Equilibrium geometries and P–Pd–P angles of hydrogen- and halogen-substituted palladium-phosphine complexes. Computed at dispersion-corrected ZORA-BLYP-D3/TZ2P

$Pd(PX_3)_2$ have nonlinear geometries. Initially, one may expect that the complexes become more linear from $Pd(PF_3)_2$ to $Pd(PI_3)_2$, based on stronger steric repulsions between the heavier halogens. We find, however, that the opposite is true: along this series the P–Pd–P angle in the equilibrium geometries decreases from 151.7° for X=F to 143.2° (X=Cl), 136.6° (X=Br), and 122.4° for X=I, as shown in Fig. 6. Furthermore, we find that $Pd(PH_3)_2$, $Pd(PF_3)_2$, $Pd(PCl_3)_2$, and $Pd(PBr_3)_2$ have eclipsed geometries, leading to a D_{3h}-symmetric geometry for $Pd(PH_3)_2$ and C_{2v}-symmetric geometries for the halogenated $Pd(PX_3)_2$ complexes. In the latter, two halogens from different ligands point towards each other. For $Pd(PI_3)_2$, we find that the ligands are rotated, avoiding close contacts between the iodines on one ligand with the iodines on the other ligand, lowering the symmetry of the complex to C_2.

It is tempting to attribute the bending of these complexes to stronger dispersion interactions between the heavier halogen substituents on different ligands, basically pulling the ligands towards each other. However, dispersion-free computations at the otherwise same ZORA-BLYP/TZ2P level reveal that also without dispersion the angles decrease steadily from 153.9° for $Pd(PF_3)_2$ to 141.6° for $Pd(PI_3)_2$ (results not shown). Thus, although dispersion contributes to the effect, it is not exclusively responsible for this nonlinearity.

We recall from previous work that sufficient π-backbonding can lead to nonlinear ML_2 geometries, because, upon bending from 180° to 90°, this π-backbonding is enhanced (see [71], as summarized in Sect. 3.4). In order to investigate the π-accepting properties of the ligands included in this work, we have performed a bond energy decomposition for the Pd–L bond in monocoordinated $PdPH_3$ and $PdPX_3$ (Table 1). We find a Pd–PH_3 bond energy of -40.9 kcal mol^{-1}, whereas the halogen-substituted phosphines bind a little stronger to Pd, with bonding energies between -43.8 and -46.1 kcal mol^{-1}. A further decomposition using Eqs. (1) and (2) reveals that, indeed, the halogen-substituted phosphines have a larger contribution from the π-component of ΔE_{oi} and hence are apparently better π-acceptors. This also follows from the lower π* orbital energies which decrease from -1.5 to -2.4, -2.7, and -3.0 eV from PF_3 to PI_3, which are all lower than that of PH_3 at -0.2 eV. However, we do not find stronger π-backbonding along the halogen-substituted series. The reason is that the π* orbital on PX_3 (which has antibonding character between P and X) is increasingly localized on the halogen substituents, and less on the phosphorus atom. Therefore, the overlap between the π* orbital and the Pd d orbitals decreases along this series, thereby counteracting the effect of the lower energy of the π* orbital. Thus, while the stronger π-backbonding for the halogen-substituted phosphines may explain

Table 1 Metal–ligand bond energies and decomposition [Eq. (2)] in kcal mol^{-1} of the monoligated $PdPX_3$ complexes

	ΔE	ΔE_{strain}	ΔE_{int}	ΔE_{disp}	ΔV_{elstat}	ΔE_{Pauli}	ΔE_{oi}	ΔE_{oi}^{σ}	ΔE_{oi}^{π}
Pd–PH_3	–40.9	+0.3	–41.2	–1.4	–165.6	+189.4	–63.6	–35.2	–28.4
Pd–PF_3	–44.4	+0.1	–44.5	–2.4	–157.8	+193.4	–77.7	–36.5	–41.3
Pd–PCl_3	–43.8	+0.1	–43.9	–5.1	–141.8	+178.8	–75.9	–34.4	–41.5
Pd–PBr_3	–45.2	+0.4	–45.6	–6.2	–133.7	+172.0	–77.7	–36.1	–41.6
Pd–PI_3	–46.1	+0.6	–46.7	–7.0	–131.0	+169.0	–77.7	–36.8	–40.9

Computed at dispersion-corrected ZORA-BLYP-D3/TZ2P

why the $Pd(PX_3)_2$ complexes are bent whereas $Pd(PH_3)_2$ is not, it does not explain the increased nonlinearity from $Pd(PF_3)_2$ to $Pd(PI_3)_2$.

We have also performed bonding analyses between ML and the second ligand, whereby we start from D_{3h}-symmetric $Pd(PH_3)_2$ or $Pd(PX_3)_2$ complexes optimized at the dispersion-free ZORA-BLYP/TZ2P level, and then bend the complex from 180° to 90° without further optimization. This way, we eliminate any geometric relaxation effects, allowing for a concise, but detailed investigation of the bonding mechanism. Thus, in Fig. 7 we show the results of the interaction energy decomposition for $Pd(PH_3)_2$ as well as the series of $Pd(PX_3)_2$ complexes. As this graph reveals, there is no significant difference between the orbital interaction curves within the halogen-substituted series. Also a further decomposition of this term into contributions from each respective irreducible representation (Eq. (3); results not shown) does not reveal any factor contributing significantly to a preference for nonlinear geometries. Figure 7 does reveal, however, that the minimum on the energy profiles shifts to smaller L–M–L angles from $Pd(PH_3)_2$ to $Pd(PF_3)_2$, and further to $Pd(PI_3)_2$, because the Pauli repulsion increases less steeply for the $Pd(PX_3)_2$ series than for $Pd(PH_3)_2$, and also along the $Pd(PX_3)_2$ series as the halogen substituents become heavier.

This, again counterintuitive, trend originates from the composition of the highest occupied MOs (HOMOs) on the L and ML fragments. The HOMO on the ligand L is the lone pair on phosphorus. For PH_3, this is the bonding combination of the hydrogen s orbitals and the phosphorus p_z orbital (with antibonding admixture of the phosphorus s orbital), which is strongly localized on phosphorus (Fig. 8). For the halogenated PX_3 ligands, the HOMO has considerably more admixture of the substituent halogen orbitals. It consists of the p_z orbitals on P and X, mixing in antibonding fashion. Thus, the larger amplitude is on the more electropositive phosphorus atom. As from F to I the halogen becomes less electronegative, this orbital becomes less localized on phosphorus (Fig. 8).

For $PdPH_3$ and $PdPX_3$, the HOMO is the antibonding combination of the ligand lone pair and the d_{z^2} orbital on Pd. Because from PH_3 to PF_3, PCl_3, PBr_3, and PI_3 the ligand lone pair becomes less localized on phosphorus, there is less destabilization from repulsions between this orbital and the palladium d_{z^2} orbital. Due to the decreased destabilization, there is less Pd 5s admixture in the $PdPH_3$ or $PdPX_3$ HOMO, resulting in the torus of the Pd d_{z^2} orbital becoming smaller (Fig. 8). It is this smaller torus from $PdPH_3$ to $PdPX_3$, and from $PdPF_3$ to $PdPI_3$, combined with the lone-pair orbital on the second ligand being less localized on phosphorus, that

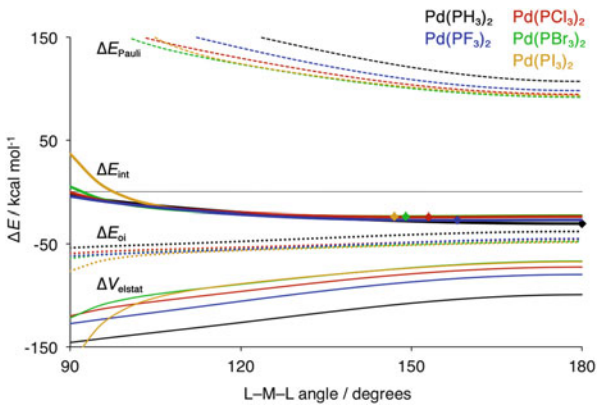

Fig. 7 Bond energy decomposition [Eq. (2)] along the L–M–L angles for $Pd(PH_3)_2$ and halogen-substituted $Pd(PX_3)_2$ complexes. *Dots* indicate the position of the minimum on the energy profile. Due to the use of frozen geometries and the omission of dispersion corrections, all minima are shifted to the right. Computed at ZORA-BLYP/TZ2P

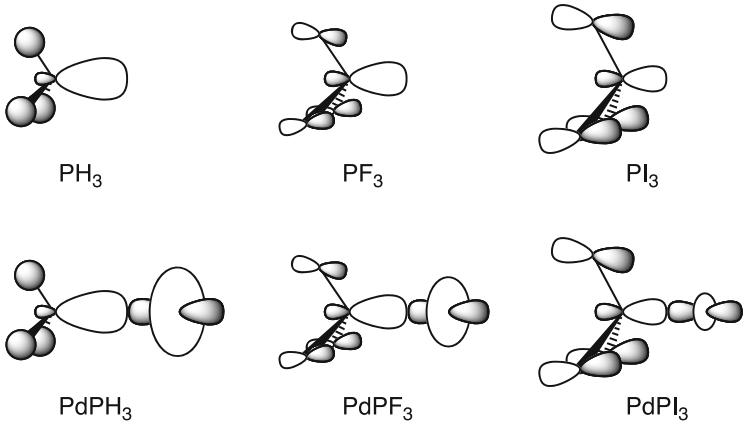

Fig. 8 Schematic representations of the HOMO on PH_3, PF_3, and PI_3 (*top*, from *left* to *right*) and on monocoordinated $PdPH_3$, $PdPF_3$, and $PdPI_3$ (*bottom*, from *left* to *right*)

results in a less steeply increasing Pauli repulsion term for the halogen-substituted catalysts compared to $Pd(PH_3)_2$, as well as along the $Pd(PX_3)_2$ series as the halogen becomes heavier (Fig. 7)

4.3 Reactivity Towards the Methane C–H Bond

For all catalytic complexes the methane C–H bond activation starts from a reactant complex (RC) that is more strongly bound along the series of catalysts, from -1.9 kcal mol^{-1} for $Pd(PH_3)_2$ to -4.7 kcal mol^{-1} for $Pd(PI_3)_2$ (Table 2 and

Table 2 Relative energies (kcal mol^{-1}) of the stationary points and transition states for methane C–H activation by the different palladium-based catalysts

	RC	TS	PC
$Pd(PH_3)_2$	–1.9	+29.5	+24.3
$Pd(PF_3)_2$	–2.8	+26.6	+24.1
$Pd(PCl_3)_2$	–3.7	+24.1	+22.1
$Pd(PBr_3)_2$	–4.4	+23.7	+22.3
$Pd(PI_3)_2$	–4.7	+25.1	+24.1

Computed at dispersion-corrected ZORA-BLYP-D3/TZ2P

Fig. 9). This is because, along this series, the catalytic complexes are bent further and therefore have a sterically less shielded metal center, allowing for a stronger substrate–catalyst interaction immediately at the beginning of the reaction. This interaction is further strengthened by increasingly stabilizing dispersion interactions between methane and the catalyst complexes with the heavier halogens.

As the reaction proceeds, a transition state (TS) is encountered at +29.5 kcal mol^{-1} for $Pd(PH_3)_2$, and at slightly lower energies for the $Pd(PX_3)_2$ series, in line with findings of previous studies [55, 57]. Along the $Pd(PX_3)_2$ series, the barriers first decrease from +26.6 kcal mol^{-1} for $Pd(PF_3)_2$ to +24.1 kcal mol^{-1} for $Pd(PCl_3)_2$ and +23.7 kcal mol^{-1} for $Pd(PBr_3)_2$, and then increase again to +25.1 kcal mol^{-1} for $Pd(PI_3)_2$.

Based on activation strain analyses along part of the reaction energy profile obtained by the Transition-Vector Approximation to the IRC (TV-IRC) [32], we find that this ordering of the barriers is the result of two counteracting trends (Fig. 10), namely a reduced strain energy from the hydrogen to the halogen substituents, and a further reduction when the halogens become heavier. The second trend is a simultaneous weakening of the interaction between the catalyst complex and methane substrate (which we address later on). Because the strain energy from $Pd(PH_3)_2$ to $Pd(PF_3)_2$ and onwards to $Pd(PI_3)_2$ decreases in progressively smaller steps, while, on the other hand, the interaction energy terms weaken with progressively larger steps, the oxidative addition barrier first decreases from $Pd(PH_3)_2$ to $Pd(PBr_3)_2$ and then increases again to $Pd(PI_3)_2$.

A further decomposition of the strain energy into individual contributions from the catalyst and substrate clearly reveals that the differences in catalyst strain are decisive. These differences are directly related to the flexibility, or indeed nonlinearity, of the complexes. Thus, although the easier bending of the L–M–L angle contributes to the progressively decreasing catalyst strain from $Pd(PH_3)_2$ to $Pd(PI_3)_2$, the potential energy surfaces for bending these complexes are very flat. The bending itself therefore only contributes a few kcal mol^{-1} to the total catalyst strain. A significant contribution to the catalyst deformation energy stems from further tilting and rotation of the ligands, which accompanies the bending. These deformations are less needed when the L–M–L angle is intrinsically more bent, and therefore add to the lowering of the catalyst strain originating from the increased flexibility of the catalyst. From $Pd(PBr_3)_2$ to $Pd(PI_3)_2$, however, this increase in flexibility is less important because it has reached a point where the catalysts are flexible enough, and the direct steric interaction between the ligands prevents further bending. This steric repulsion is also revealed in Fig. 7 by the strong

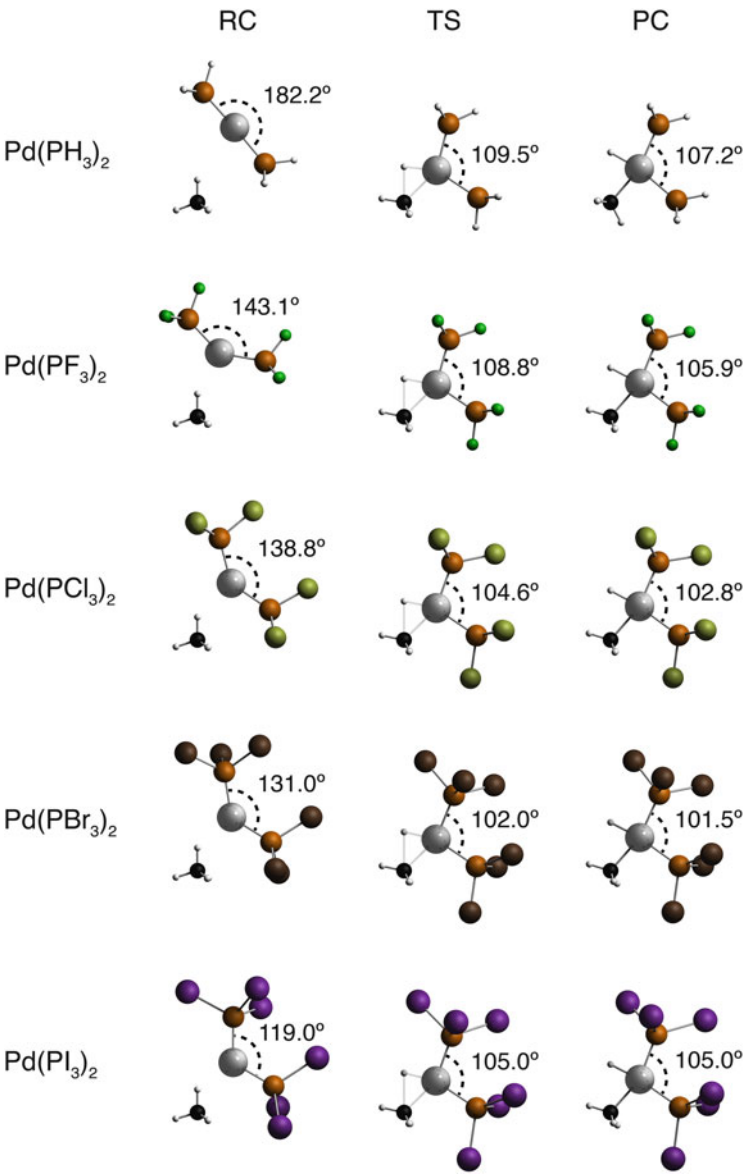

Fig. 9 Geometries of the RC, TS, and PC along the energy profile for oxidative addition of methane to $Pd(PH_3)_2$, $Pd(PF_3)_2$, $Pd(PCl_3)_2$, $Pd(PBr_3)_2$, and $Pd(PI_3)_2$. Computed at dispersion-corrected ZORA-BLYP-D3/TZ2P

increase in Pauli repulsion that occurs at angles below 110°. Although only the beginning of this sharp increase of the Pauli repulsion term is visible in the graph and most of it is off the scale, its effect (even though partly masked by the more

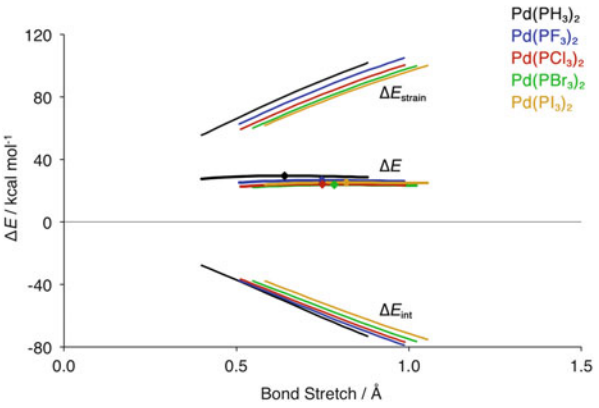

Fig. 10 Activation strain analyses [Eq. (1)] along partial energy profiles for $Pd(PH_3)_2$ and $Pd(PX_3)_2$, obtained by the TV-IRC method. Computed at dispersion-corrected ZORA-BLYP-D3/TZ2P

stabilizing electrostatic attraction and orbital interactions) is still clearly visible in the total interaction energy curve. Due to this direct ligand–ligand repulsion, the bite angle does not decrease any further from the TS to the PC of addition to $Pd(PI_3)_2$, but retains a value of 105.0°, slightly larger than for $Pd(PBr_3)_2$ (see Fig. 9).

Finally, we address the progressively weaker interaction between the fragments. From $Pd(PH_3)_2$ to the series of halogen-substituted catalysts, the interaction weakens mainly due to a less stabilizing orbital interaction term. This is caused by weaker catalyst-to-substrate backbonding, due to a lower orbital energy of the donating orbitals on the halogenated catalysts. The reason for these lower orbital energies is the better π-backdonation to the halogenated phosphine ligands (Table 1). This stronger backdonation generates a more positive potential on the Pd center, which stabilizes the donating orbitals. This is accompanied by the fact that, upon bending, the HOMO on the catalyst is pushed up less in energy, because from PH_3 to the halogen-substituted PX_3, the lone pairs are less localized on the phosphorus atom (see Sect. 4.2 and Fig. 8) and therefore have a weaker antibonding interaction with the palladium d orbitals.

Along the halogenated series, from $Pd(PF_3)_2$ to $Pd(PI_3)_2$, the orbital interaction term is remarkably similar, and the weakening of the catalyst–substrate interaction along this series results from an increasing Pauli repulsion. This destabilizing term is strengthened along this series because, from $Pd(PF_3)_2$ to $Pd(PI_3)_2$, there are more orbitals on the catalyst with energies in the vicinity of the methane HOMO energy, and therefore an increasingly large number of occupied catalyst orbitals enter a 2-center, 4-electron repulsion with the methane HOMO [87].

4.4 Conclusions and Outlook

Halogen-substituted palladium-phosphine complexes $Pd(PX_3)_2$ with X=F, Cl, Br, or I all have nonlinear geometries, unlike $Pd(PH_3)_2$ which has a linear ligand–metal–ligand angle. Along the $Pd(PX_3)_2$ series the ligand–metal–ligand angle

decreases from 151.7° for $Pd(PF_3)_2$, to 143.2°, 136.6°, and 122.4° for $Pd(PCl_3)_2$, $Pd(PBr_3)_2$, and $Pd(PI_3)_2$, respectively. This follows from dispersion-corrected relativistic density functional computations. We found that the nonlinearity is the result of a combination of factors: firstly, the potential energy surfaces for bending the halogenated phosphine complexes are flat due to the increased π-backbonding that occurs upon bending from 180° to 90°. Secondly, from $Pd(PH_3)_2$ to $Pd(PF_3)_2$ and onwards to $Pd(PI_3)_2$, there is a less steeply increasing Pauli repulsion between $PdPH_3$ or $PdPX_3$ and the second ligand due to a smaller overlap of the highest occupied MOs upon bending. Thirdly, as along the $Pd(PX_3)_2$ series the halogen substituents become heavier, the stronger dispersion interactions between the ligands pull them more closely to each other.

When applied as catalytic complexes for methane C–H bond activation, this nonlinearity leads to a lower reaction barrier for the halogenated catalysts $Pd(PX_3)_2$ compared to $Pd(PH_3)_2$, because there is less deformation energy needed to bend away the ligands in order to make room for the approaching methane. Along the $Pd(PX_3)_2$ series, there are two opposing trends, resulting in lower barriers from $Pd(PF_3)_2$ to $Pd(PBr_3)_2$, but a slightly higher barrier for $Pd(PI_3)_2$. The two trends are: (1) a less destabilizing catalyst strain energy due to increased nonlinearity; counteracted by (2) a less stabilizing interaction energy due to a larger number of repulsive occupied–occupied orbital interactions. From $Pd(PBr_3)_2$ to $Pd(PI_3)_2$ this latter trend outweighs the effect of the decreased strain energy.

We envisage that the insights discussed in this chapter provide chemists with better design principles, and therefore contribute to a more rational fragment-oriented design of catalysts.

References

1. Diederich F, Stang PJ (1998) Metal-catalyzed cross-coupling reactions. Weinheim, Wiley-VCH
2. Hartwig JF (2010) Organotransition metal chemistry: from bonding to catalysis, 1st edn. University Science Books, Sausalito
3. The Nobel Prize in Chemistry (2010) Press Release. Nobelprize.org. http://nobelprize.org/nobel_prizes/chemistry/laureates/2010/press.html. 6 Oct 2010
4. Suzuki A (2011) Cross-coupling reactions of organoboranes: an easy way to construct C–C bonds (Nobel lecture). Angew Chem Int Ed 50:6722
5. Negishi E-I (2011) Magical power of transition metals: past, present, and future (Nobel lecture). Angew Chem Int Ed 50:6738
6. Shilov AE, Shul'pin GB (1997) Activation of C–H bonds by metal complexes. Chem Rev 97:2879
7. Beletskaya IP, Cheprakov AV (2000) The Heck reaction as a sharpening stone of palladium catalysis. Chem Rev 100:2009
8. Van Der Boom ME, Milstein D (2003) Cyclometalated phosphine-based pincer complexes: mechanistic insight in bond activation. Chem Rev 103:1759
9. Crabtree RH (2004) Organometallic alkane CH activation. J Organomet Chem 689:4083
10. Weisshaar JC (1993) Bare transition metal atoms in the gas phase: reactions of M, M^+, and M^{2+} with hydrocarbons. Acc Chem Res 26:213

11. Ziegler T (1991) Approximate density functional theory as a practical tool in molecular energetics and dynamics. Chem Rev 91:651
12. Niu SQ, Hall MB (2000) Theoretical studies on reactions of transition-metal complexes. Chem Rev 100:353
13. Torrent M, Solà M, Frenking G (2000) Theoretical studies of some transition-metal-mediated reactions of industrial and synthetic importance. Chem Rev 100:439
14. Dedieu A (2000) Theoretical studies in palladium and platinum molecular chemistry. Chem Rev 100:543
15. Diefenbach A, De Jong GT, Bickelhaupt FM (2005) Fragment-oriented design of catalysts based on the activation strain model. Mol Phys 103:995
16. Bickelhaupt FM (1999) Understanding reactivity with Kohn–Sham molecular orbital theory: E2-S_N2 mechanistic spectrum and other concepts. J Comp Chem 20:114
17. Diefenbach A, De Jong GT, Bickelhaupt FM (2005) Activation of H–H, C–H, C–C and C–Cl bonds by Pd and $PdCl^-$. Understanding anion assistance in C–X bond activation. J Chem Theory Comput 1:286
18. De Jong GT, Bickelhaupt FM (2007) Transition-state energy and position along the reaction coordinate in an extended activation strain model. ChemPhysChem 8:1170
19. Van Zeist W-J, Bickelhaupt FM (2010) The activation strain model of chemical reactivity. Org Biomol Chem 8:3118
20. Amatore C, Jutand A (1999) Mechanistic and kinetic studies of palladium catalytic sytems. J Organomet Chem 576:254
21. Kozuch S, Amatore C, Jutand A, Shaik S (2005) What makes for a good catalytic cycle? A theoretical study of the role of an anionic palladium(0) complex in the cross-coupling of an aryl halide with an anionic nucleophile. Organometallics 24:2319
22. Kozuch S, Shaik S (2011) How to conceptualize catalytic cycles? The energetic span model. Acc Chem Res 44:101
23. Kozuch S (2012) A refinement of everyday thinking: the energetic span model for kinetic assessment of catalytic cycles. WIREs Comput Mol Sci 2:795
24. Legault CY, Garcia Y, Merlic CA, Houk KN (2007) Origin of regioselectivity in palladium-catalyzed cross-coupling reactions of polyhalogenated heterocycles. J Am Chem Soc 129:12664
25. Galabov B, Nikolova V, Wilke JJ, Schaefer HF III, Allen WD (2008) Origin of the S_N2 benzylic effect. J Am Chem Soc 130:9887
26. Bento AP, Bickelhaupt FM (2008) Nucleophilicity and leaving-group ability in frontside and backside S_N2 reactions. J Org Chem 73:7290
27. Ess DH, Houk KN (2008) Theory of 1,3-dipolar. Cycloadditions: distortion/interaction and frontier molecular orbital models. J Am Chem Soc 130:10187
28. Wolters LP, Bickelhaupt FM (2012) Halogen bonding versus hydrogen bonding: a molecular orbital perspective. Chem Open 1:96
29. Bickelhaupt FM, Baerends EJ (2003) The case for steric repulsion causing the staggered conformation of ethane. Angew Chem Int Ed 42:4183
30. Poater J, Sola M, Bickelhaupt FM (2006) Hydrogen-hydrogen bonding in planar biphenyl, predicted by atoms-in-molecules theory, does not exist. Chem Eur J 12:2889
31. Fernández I, Bickelhaupt FM, Cossío FP (2012) Type-I dyotropic reactions: understanding trends in barriers. Chem Eur J 18:12395
32. Van Zeist W-J, Koers AH, Wolters LP, Bickelhaupt FM (2008) Reaction coordinates and the transition-vector approximation to the IRC. J Chem Theory Comput 4:920
33. Bickelhaupt FM, Baerends EJ (2000) Kohn–Sham density functional theory: predicting and understanding chemistry. In: Lipkowitz KB, Boyd DB (eds) Reviews in computational chemistry. Wiley-VCH, New York
34. Baerends EJ, Gritsenko OV (1997) A quantum chemical view of density functional theory. J Phys Chem A 101:5383

35. Ziegler T, Rauk A (1979) A theoretical study of the ethylene-metal bond in complexes between Cu^+, Ag^+, Au^+, Pt^0 or Pt^{2+} and ethylene, based on the Hartree–Fock–Slater transition-state method. Inorg Chem 18:1558
36. Te Velde G, Bickelhaupt FM, Baerends EJ, Fonseca GC, Van Gisbergen SJA, Snijders JG, Ziegler T (2001) Chemistry with ADF. J Comput Chem 22:931
37. Fonseca GC, Snijders JG, Te Velde G, Baerends EJ (1998) Towards an order-N DFT method. Theor Chem Acc 99:391
38. Baerends EJ, Ziegler T, Autschbach J, Bashford D, Bérces A, Bickelhaupt FM, Bo C, Boerrigter PM, Cavallo L, Chong DP, Deng L, Dickson RM, Ellis DE, Van Faassen M, Fan L, Fischer TH, Fonseca Guerra C, Ghysels A, Giammona A, Van Gisbergen SJA, Götz AW, Groeneveld JA, Gritsenko OV, Grüning M, Gusarov S, Harris FE, Van Den Hoek P, Jacob CR, Jacobson H, Jensen L, Kaminski JW, Van Kessel G, Kootstra F, Kovalenko A, Krykunov MV, Van Lenthe E, McCormack DA, Michalak A, Mitoraj M, Neugebauer J, Nicu VP, Noodleman L, Osinga VP, Patchkovskii S, Philipsen PHT, Post D, Pye CC, Ravenek W, Rodríguez JI, Ros P, Schipper PRT, Schreckenbach G, Seldenthuis JS, Seth M, Snijders JG, Solà M, Swart M, Swerhone D, Te Velde G, Vernooijs P, Versluis L, Visscher L, Visser O, Wang F, Wesolowski TA, Van Wezenbeek EM, Wiesenekker G, Wolff SK, Woo TK, Yakovlev AL, SCM, Theoretical Chemistry; Vrije Universiteit, Amsterdam, The Netherlands. http://www.scm.com/
39. Van Zeist W-J, Fonseca GC, Bickelhaupt FM (2008) PyFrag – streamlining your reaction path analysis. J Comput Chem 29:312
40. Diefenbach A, Bickelhaupt FM (2004) Activation of H–H, C–H, C–C, and C–Cl Bonds by Pd(0). Insight from the activation strain model. J Phys Chem A 108:8460
41. De Jong GT, Kovács A, Bickelhaupt FM (2006) Oxidative addition of hydrogen halides and dihalogens to Pd. Trends in reactivity and relativistic effects. J Phys Chem A 110:7943
42. Diefenbach A, Bickelhaupt FM (2005) Activation of C–H, C–C and C–I bonds by Pd and cis-$Pd(CO)_2I_2$. Catalyst–substrate adaptation. J Organomet Chem 690:2191
43. De Jong GT, Bickelhaupt FM (2007) Catalytic carbon–halogen bond activation: trends in reactivity, selectivity, and solvation. J Chem Theory Comput 3:514
44. Low JJ, Goddard WA III (1986) Theoretical studies of oxidative addition and reductive elimination. 2. Reductive coupling of H–H, H–C, and C–C bonds from palladium and platinum complexes. Organometallics 5:609
45. Low JJ, Goddard WA III (1986) Theoretical studies of oxidative addition and reductive elimination. 3. C–H and C–C reductive coupling from palladium and platinum bis(phosphine) complexes. J Am Chem Soc 108:6115
46. Blomberg MRA, Brandemark U, Siegbahn PEM (1983) Theoretical investigation of the elimination and addition reactions of methane and ethane with nickel. J Am Chem Soc 105:5557
47. Siegbahn PEM, Blomberg MRA (1992) Theoretical study of the activation of C–C bonds by transition metal atoms. J Am Chem Soc 114:10548
48. Saillard JY, Hoffmann R (1984) C–H and H–H activation in transition-metal complexes and on surfaces. J Am Chem Soc 106:2006
49. Forster D (1975) Halide catalysis of the oxidative addition of alkyl halides to rhodium (1) complexes. J Am Chem Soc 97:951
50. Blomberg MRA, Schüle J, Siegbahn PEM (1989) Ligand effects on metal-R bonding, where R is hydrogen or alkyl. A quantum chemical study. J Am Chem Soc 111:6156
51. Amatore C, Jutand A, Suarez A (1993) Intimate mechanism of oxidative addition to zerovalent palladium complexes in the presence of halide-ions and its relevance to the mechanism of palladium-catalyzed nucleophilic substitutions. J Am Chem Soc 115:9531
52. Siegbahn PEM, Blomberg MRA (1994) Halide ligand effects on the oxidative addition reaction of methane and hydrogen to second row transition metal complexes. Organometallics 13:354

53. Amatore C, Jutand A (2000) Anionic Pd(0) and Pd(II) intermediates in palladium-catalyzed heck and cross-coupling reactions. Acc Chem Res 33:314
54. Hammond GS (1955) A correlation of reaction rates. J Am Chem Soc 77:334
55. Fazaeli R, Ariafard A, Jamshidi S, Tabatabaie ES, Pishro KA (2007) Theoretical studies of the oxidative addition of PhBr to $Pd(PX_3)_2$ and $Pd(X_2PCH_2CH_2PX_2)$ (X=Me, H, Cl). J Organomet Chem 692:3984
56. Van Zeist W-J, Visser R, Bickelhaupt FM (2009) The steric nature of the bite angle. Chem Eur J 15:6112
57. Van Zeist W-J, Bickelhaupt FM (2011) Steric nature of the bite angle. A closer and a broader look. Dalton Trans 40:3028
58. Jover J, Fey N, Purdie M, Lloyd-Jones GC, Harvey JN (2010) A computational study of phosphine ligand effects in Suzuki–Miyaura coupling. J Mol Catal A Chem 324:39
59. Besora M, Gourlaouen C, Yates B, Maseras F (2011) Phosphine and solvent effects on oxidative addition of CH_3Br to $Pd(PR_3)$ and $Pd(PR_3)_2$ complexes. Dalton Trans 40:11089
60. Su M, Chu S (1998) Theoretical study of oxidative addition and reductive elimination of 14-electron d^{10} ML_2 complexes: a $ML_2 + CH_4$ (M=Pd, Pt; L=CO, PH_3, L_2=$PH'_2CH_2CH_2PH_2$) case study. Inorg Chem 37:3400
61. Dierkes P, Van Leeuwen PWNM (1999) The bite angle makes the difference: a practical ligand parameter for diphosphine ligands. J Chem Soc Dalton 1999:1519–1529
62. Van Leeuwen PWNM, Kamer P, Reek JNH, Dierkes P (2000) Ligand bite angle effects in metal-catalyzed C–C bond formation. Chem Rev 100:2741
63. Freixa Z, Van Leeuwen PWNM (2003) Bite angle effects in diphosphine metal catalysts: steric or electronic? Dalton T 2003:1890
64. Birkholz (née Gensow) M-N, Freixa Z, Van Leeuwen PWNM (2009) Bite angle effects of diphosphines in C–C and C–X bond forming cross coupling reactions. Chem Soc Rev 38:1099
65. Hofmann P, Heiss H, Müller G (1987) Synthesis and molecular-structure of dichloro[η^2-bis (di-*t*-butylphosphino)methane]platinum(II), $Pt(dtbpm)Cl_2$. The electronic structure of 1,3-diphosphaplatinacyclobutane fragments. Z Naturforsch 42b:395
66. Koga N, Morokuma K (1991) Ab initio molecular orbital studies of catalytic elementary reactions and catalytic cycles of transition-metal complexes. Chem Rev 91:823
67. Eller K, Schwarz H (1991) Organometallic chemistry in the gas phase. Chem Rev 91:1121
68. Wittborn ACM, Costas M, Blomberg MRA, Siegbahn PEM (1997) The C–H activation reaction of methane for all transition metal atoms from the three transition rows. J Chem Phys 107:4318–4328
69. De Jong GT, Bickelhaupt FM (2009) Bond activation by group-11 transition-metal cations. Can J Chem 87:806
70. Wolters LP, Van Zeist W-J, Bickelhaupt FM (2014) d-regime, s-regime and intrinsic bite-angle flexibility: new concepts for designing d^{10}-ML_n catalysts. Submitted for publication
71. Wolters LP, Bickelhaupt FM (2013) Nonlinear d^{10}-ML_2 transition-metal complexes. Chem Open 2:106
72. Otsuka S (1980) Chemistry of platinum and palladium compounds of bulky phosphines. J Organomet Chem 200:191
73. Ziegler T (1985) Theoretical study on the stability of $M(PH_3)_2(O_2)$, $M(PH_3)_2(C_2H_2)$, and $M(PH_3)_2(C_2H_4)$ (M=Ni, Pd, Pt) and $M(PH_3)_4(O_2)^+$, $M(PH_3)_4(C_2H_2)^+$, and $M(PH_3)_4(C_2H_4)^+$ (M=Co, Rh, Ir) by the HFS-transition-state method. Inorg Chem 24:1547
74. King RB (2000) Atomic orbitals, symmetry, and coordination polyhedra. Coord Chem Rev 197:141
75. Carvajal MA, Novoa JJ, Alvarez S (2004) Choice of coordination number in d^{10} complexes of group 11 metals. J Am Chem Soc 126:1465
76. Albright TA, Burdett JK, Whangbo MH (2013) Orbital interactions in chemistry, 2nd edn. Wiley, New York
77. Zhou M, Andrews L (1998) Matrix infrared spectra and density functional calculations of $Ni(CO)_x^-$, $x = 1$–3. J Am Chem Soc 120:11499

78. Manceron L, Alikhani ME (1999) Infrared spectrum and structure of $Ni(CO)_2$ – a matrix isolation and DFT study. Chem Phys 244:215
79. Jolly CA, Marynick DS (1989) Ground-state geometries and inversion barriers for simple complexes of early transition metals. Inorg Chem 28:2893
80. Kaupp M (2001) "Non-VSEPR" structures and bonding in d0 systems. Angew Chem Int Ed 40:3534
81. Gillespie RJ, Bytheway I, DeWitte RS, Bader RFW (1994) Trigonal bipyramidal and related molecules of the main group elements: investigation of apparent exceptions to the VSEPR model through the analysis of the laplacian of the electron density. Inorg Chem 33:2115
82. Kaupp M, Schleyer PVR (1992) The structural variations of monomeric alkaline earth MX_2 compounds (M=Ca, Sr, Ba; X = Li, BeH, BH_2, CH_3, NH_2, OH, F). An ab initio pseudopotential study. J Am Chem Soc 114:491
83. Kaupp M (1999) On the relation between π bonding, electronegativity, and bond angles in high-valent transition metal complexes. Chem Eur J 5:3631
84. Ogasawara M, Macgregor SA, Streib WE, Folting K, Eisenstein O, Caulton KG (1995) Isolable, unsaturated Ru(0) in $Ru(CO)_2(P^tBu_2Me)_2$: not isostructural with Rh(I) in $Rh(CO)_2(PR_3)_2^+$. J Am Chem Soc 117:8869
85. Ogasawara M, Macgregor SA, Streib WE, Folting K, Eisenstein O, Caulton KG (1996) Characterization and reactivity of an unprecedented unsaturated zero-valent ruthenium species: isolable, yet highly reactive. J Am Chem Soc 118:10189
86. Grimme S, Antony J, Ehrlich S, Krieg H (2010) A consistent and accurate ab initio parametrization of density functional dispersion correction (DFT-D) for the 94 elements H-Pu. J Chem Phys 132:154104
87. Bickelhaupt FM, DeKock RL, Baerends EJ (2002) The short N–F bond in N_2F^+ and how Pauli repulsion influences bond lengths. Theoretical study of N_2X^+, NF_3X^+, and NH_3X^+ (X = F, H). J Am Chem Soc 124:1500